Chromophore-Modified Bisnaphthalimides: DNA Recognition, Topoisomerase Inhibition, and Cytotoxic Properties of Two Mono- and Bisfuronaphthalimides†

Christian Bailly,*,‡ Carolina Carrasco,‡ Alexandra Joubert,‡ Christine Bal,‡ Nicole Wattez,‡ Marie-Paule Hildebrand,‡ Amélie Lansiaux,‡ Pierre Colson,§ Claude Houssier,§ Monica Cacho,|| Ana Ramos,|| and Miguel F. Braña||

INSERM U-524 et Laboratoire de Pharmacologie Antitumorale du Centre Oscar Lambret, IRCL, Place de Verdun, 59045 Lille, France, Biospectroscopy and Physical Chemistry Unit, Department of Chemistry and Natural and Synthetic Drugs Research Center, University of Liege, Sart-Tilman, 4000 Liege, Belgium, and Departamento de CC. Químicas, Facultad de CC Experimentales y de la Salud, Universidad San Pablo-CEU, Urb. Montepríncipe, Boadilla del Monte, 28668 Madrid, Spain

Received December 23, 2002; Revised Manuscript Received February 17, 2003

ABSTRACT: Bisnaphthalimides represent a promising group of DNA-targeted anticancer agents. In this series, the lead compounds elinafide and bisnafide have reached clinical trials, and the search for more potent analogues remains a priority. In the course of a medicinal chemistry program aimed at discovering novel antitumor drugs based on the naphthalimide skeleton, different dimeric molecules containing two tetracyclic neutral DNA intercalating chromophores were synthesized. The naphthalimide unit has been fused to a benzene ring (azonafide derivatives), an imidazole, a pyrazine, or, as reported here, a furan ring which increases the planar surface of the chromophore and enhances its stacking properties. We report a detailed investigation of the DNA binding capacity of the dimeric molecule **MCI3335** composed of two furonaphthalimide units connected by a 12 Å long amino alkyl linker [$(CH_2)_2$-NH-$(CH_2)_3$-NH-$(CH_2)_2$] identical to that of elinafide. Qualitative and quantitative binding studies, in particular using surface plasmon resonance, establish that the dimer binds considerably more tightly to DNA (up to 1000 times) than the corresponding monomer and exhibits a higher sequence selectivity for GC-rich sequences. DNase I footprinting experiments attest that the dimer, and to a lesser extent the monomer, preferentially intercalate at GC sites. The strong binding interaction between the drugs and DNA perturbs the relaxation of supercoiled DNA by topoisomerases, but the test compounds do not promote DNA cleavage by topoisomerase I or II. Despite the lack of poisoning effect toward topoisomerase II, **MCI3335** displays a very high cytotoxicity toward CEM human leukemia cells, with an IC_{50} in the low nanomolar range, ∼4 times inferior to that of the reference drug elinafide. Confocal microscopy observations indicate that the monomer shows a stronger tendency to accumulate in the cell nuclei than the dimer. The extremely high cytotoxic potential of **MCI3335** is attributed to its enhanced capacity to bind to DNA and to inhibit DNA synthesis, as evidenced by flow cytometry experiments using the BrdU assay. The results provide novel mechanistic information that furthers the understanding of the structure−activity relationships in the bisnaphthalimide series and identify **MCI3335** as a novel lead compound for further preclinical investigations.

Bisnaphthalimides represent a group of promising antitumor agents targeting DNA and topoisomerases (*1*−*3*). These compounds bear two intercalating tricyclic ring systems connected by a linker of variable length and rigidity. The lead compounds in the series are the drugs called bisnafide (DMP-840) (*4*−*6*) and elinafide (LU 79553) (*7*) which have been tested in the clinic for the treatment of solid tumors (*8*−*12*). They contain the same naphthalimide units but differ in the structure of the linker between the two imide functions (Figure 1). The aminoalkyl linker chain found in elinafide [$(CH_2)_2$-NH-$(CH_2)_3$-NH-$(CH_2)_2$] separates the two chromophores by ∼12.3 Å [N−N distance for the fully extended form estimated by computer modeling (*13*)], and this is sufficient to allow both moieties to intercalate into DNA (*14*, *15*). An interchromophore separation of 9−13 Å is usually considered necessary to permit two planar ring systems to sandwich two base pairs in the intercalated complex (*16*).

Mononaphthalimide derivatives also provide potent antitumor agents. In this series, the lead compounds are the amino and nitro derivatives amonafide and mitonafide (Figure 1) which have also been tested clinically (*17*−*21*).

† This work was supported by grants from the Association pour la Recherche sur le Cancer (to C. Bailly), from Fundacion Ramon Areces (to M.C.), and from the DEGS (MEC-Spain, Grant PB98-0055) and the Universidad San Pablo-CEU (Grant 5-99/00 U.S.P.) (to M.F.B.). C.C. was the recipient of a Marie Curie Fellowship of the European Community Program "Improving Human Research Potential and the Socio-economic Knowledge Base" under Contract HPMFCT-2000-00701. Support by the "Actions intégrées Franco-Belge, Program Tournesol" is acknowledged.

* To whom correspondence should be addressed: INSERM U-524, IRCL, Place de Verdun, 59045 Lille, France. E-mail: bailly@lille.inserm.fr.

‡ IRCL.

§ University of Liege.

|| Universidad San Pablo-CEU.

10.1021/bi027415c CCC: $25.00
Published on Web 03/21/2003

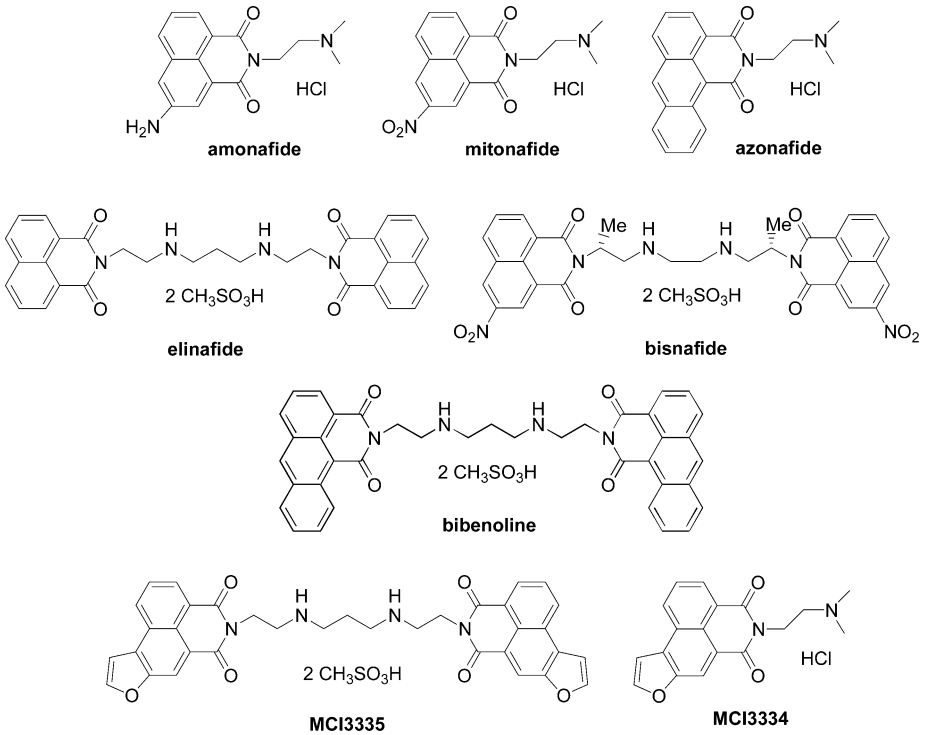

FIGURE 1: Structures of amonafide, mitonafide, azonafide, elinafide (LU 79553), bisnafide (DMP-840), and the two compounds used in this study.

Various attempts have been made to modify the naphthalimide unit to reinforce its DNA binding capacity. In the monomer series, the substitution of an anthracene for the naphthalene leads to the development of the drug azonafide (Figure 1) which was found to be more cytotoxic than amonafide (*22*, *23*), presumably because of the higher affinity of azonafide for DNA than of amonafide (*24*).

Dimers of azonafide have also been designed, and the bisdibenz[*de*,*h*]isoquinoline-1,3-dione derivative incorporating the aforementioned $(CH_2)_2$-NH-$(CH_2)_3$-NH-$(CH_2)_2$ bridge was found to be extremely efficient against melanoma in vivo (*25*, *26*). This compound, now designated bibenoline (Figure 1), has been selected for preclinical development. More recently, various analogues containing an imidazole (*27*) or a pyrazine (*28*) ring fused to the naphthalene moiety were synthesized and evaluated as cytotoxic agents. Here again, bisintercalation was clearly established for the compounds possessing the linker indicated above. Highly cytotoxic agents were found in the pyrazine series, encouraging the search for novel drug candidates in the bisnaphthalimide series.

DNA and topoisomerases represent privileged targets for all these naphthalimide compounds. The topoisomerase II inhibitory activity of amonafide and mitonafide has been extensively characterized (*29*−*32*). Bisnafide also kills eukaryotic cells by stabilizing the cleavage complex of topoisomerase II with DNA (*33*), and elinafide has also been shown to interfere with the activity of topoisomerase II (*7*), although in this case cell killing is likely due to the inhibition of other enzymes and/or transcription factors that act on DNA (*13*). DNA is obviously an ideal bioreceptor for all these mono- and bisnaphthalimide derivatives. The capacity of amonafide and mitonafide to form intercalation complexes has long been recognized (*34*). The propensity of elinafide to bisintercalate into duplex DNA has also been firmly established on the basis of biochemical (viscometric) (*14*) and spectroscopy (NMR) data (*15*). Interestingly, the two studies independently indicated that the aminoalkyl linker chain connecting the two naphthalimide units resides in the major groove of DNA to establish molecular contacts with GC base pairs.

In our continued efforts to develop DNA-binding antitumor agents, we report here the synthesis (Scheme 1) and molecular pharmacology of two novel naphthalimides containing one or two furonaphthalimide chromophores (Figure 1). The monomeric compound **4** (**MCI3334**) bears a dimethylaminoethyl chain identical to that of amonafide and mitonafide. The aforementioned $(CH_2)_2$-NH-$(CH_2)_3$-NH-$(CH_2)_2$ bridge has been preserved to build the dimeric compound **5** (**MCI3335**). The DNA binding characteristics of these two molecules were examined using a range of biochemical and biophysical methods, and their effects on DNA topoisomerases and cytotoxic potential were investigated.

MATERIALS AND METHODS

Chemistry. The synthesis of anhydride **3**, from which naphthalimides **4** (**MCI3334**) and **5** (**MCI3335**) were prepared, was carried out following the method described by Patten (*35*) and outlined in Scheme 1. Thus, dimethyl homophthalate was treated with 2-furaldehyde in the presence of NaH to yield ester **2**. Irradiation of this latter one in the presence of I_2 brought about the oxidative photocyclization of the stylbene type system. The product formed was not isolated, but it was directly converted into the corresponding anhydride **3** by hydrolysis of the ester group present in the molecule (1 M NaOH), followed by dehydration (Ac_2O/Δ). Mononaphthalimide **4** was synthesized by treatment of **3** with an equimolecular amount of *N*,*N*-dimethyl-1,2-ethanediamine in EtOH and toluene at reflux temperature. Bisnaphthalimide

Scheme 1[a]

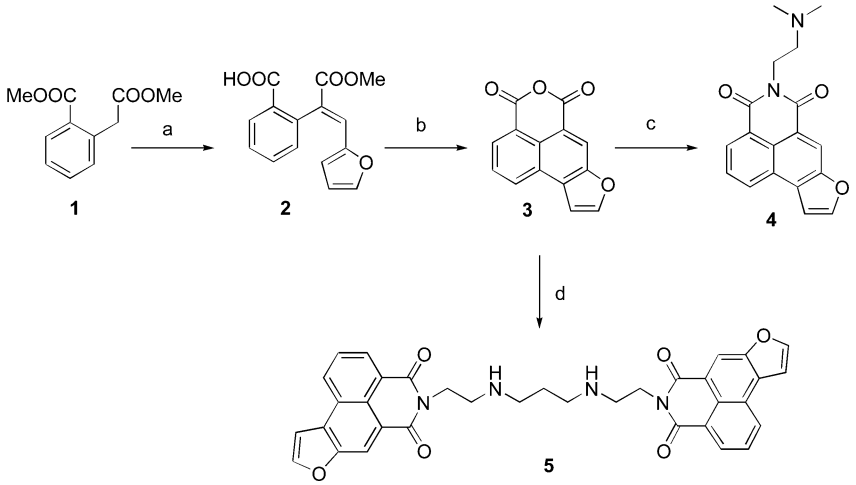

[a] (a) 2-Furaldehyde in THF, then NaH (80%); (b) (i) $I_2/h\nu$, EtOH, (ii) 1 M NaOH, (iii) saturated $NaHSO_3$, (iv) Ac_2O, Δ; (c) $NH_2(CH_2)_2N(CH_3)_2$; (d) $NH_2(CH_2)_2NH(CH_2)_3NH(CH_2)_2NH_2$.

5 was obtained by a similar procedure, starting from **3** and *N*,*N*′-bis(2-aminoethyl)-1,3-propanediamine in a 2:1 ratio. Except for the SPR experiments, the drugs were dissolved in DMSO at 5 mM. The stock DMSO solutions of drugs were kept at −20 °C and freshly diluted with water to the desired concentration immediately prior to use. For the SPR experiments, the furonaphthalimides (methanesulfonate salts) were directly dissolved in water.

Experimental. Melting points (uncorrected) were determined on a Stuart Scientific SMP3 apparatus. Infrared (IR) spectra were recorded with a Perkin-Elmer 1330 infrared spectrophotometer. ^{1}H and ^{13}C NMR spectra were recorded on a Bruker 300-AC instrument. Chemical shifts (δ) are expressed in parts per million relative to internal tetramethylsilane; coupling constants (*J*) are in hertz. Mass spectra were recorded on an HP 5989A spectrometer. Elemental analyses (C, H, N) were performed on a Perkin-Elmer 2400 CHN apparatus at the Microanalyses Service of the University Complutense of Madrid (Madrid, Spain); unless otherwise stated, all reported values are within ±0.4% of the theoretical compositions. Thin-layer chromatography (TLC) was carried out on Merck silica gel 60 F-254 plates. Unless stated otherwise, starting materials were high-grade commercial products.

*(1) 5-[2-(Dimethylamino)ethyl]benz[de]furo[3,2-g]isoquinoline-4,6(5H)-dione (**4**)*. A suspension of **3** (80 mg, 0.34 mmol) in toluene (3 mL) was treated with *N*,*N*-dimethylethylenediamine (29 mg, 0.34 mmol) in absolute EtOH (0.5 mL). The mixture was heated at reflux temperature until the reaction was completed (TLC). The precipitated solid was filtered and recrystallized from absolute EtOH and toluene to provide mononaphthalimide **1** (74 mg, 70%) as a yellow solid: mp 180−183 °C; IR (KBr) 1680, 1650 cm^{-1}; ^{1}H NMR (CF_3CO_2D) δ 8.96 (s, 1H, ArH), 8.83 (d, 1H, J = 8.7, ArH), 8.77 (d, 1H, J = 7.4, ArH), 8.21 (s, 1H, ArH), 8.05 (m, 1H, ArH), 7.58 (s, 1H, ArH), 4.89 (br s, 2H, CH_2), 3.85 (br s, 2H, CH_2), 3.28 (s, 6H, $2CH_3$). A suspension of the free base (95 mg, 0.31 mmol) in absolute EtOH (10 mL) was saturated with HCl (g) for 2 h, and the solid that formed was filtered to give the corresponding HCl·1.5H_2O (76 mg, 71%): mp >300 °C; IR (KBr) 2550, 2450, 1690, 1655 cm^{-1}; ^{1}H NMR (D_2O) δ 7.66 (m, 1H, FuranH), 7.48 (d, 1H, J = 7.7, ArH), 7.41 (d, 1H, J = 8.2, ArH), 7.26 (s, 1H, ArH), 7.01 (dd, 1H, J = 8.2 and 7.7, ArH), 6.67 (m, 1H, FuranH), 3.88 (t, 2H, J = 6.6, CH_2), 3.10 (t, 2H, J = 6.6, CH_2), 2.79 (s, 6H, $2CH_3$); ^{13}C NMR (D_2O) δ 165.2, 164.8, 151.23, 151.18, 131.5, 130.4, 130.2, 127.7, 125.2, 123.8, 120.5, 117.0, 116.4, 107.0, 55.7, 44.2, 36.1. Anal. ($C_{18}H_{16}N_2O_3$·HCl·1.5H_2O) C, H, N.

*(2) N,N′-Bis[2-(4,6-dioxo-5,6-dihydro-4H-benz[de]furo-[3,2-g]isoquinolin-5-yl)ethyl]-1,3-propanediamine (**5**)*. A suspension of anhydride **3** (227 mg, 0.95 mmol) in toluene (5 mL) was treated with *N*,*N*′-bis(2-aminoethyl)-1,3-propanediamine (77 mg, 0.48 mmol) in absolute EtOH (2 mL). The mixture was heated at reflux temperature until the reaction was completed (TLC). The precipitated solid was filtered and recrystallized from absolute EtOH and toluene to provide bisnaphthalimide **5** (241 mg, 84%) as a yellow solid: mp 167−168 °C; IR (KBr) 3400, 1685, 1645 cm^{-1}; ^{1}H NMR (CF_3CO_2D) δ 8.89 (br s, 2H, ArH), 8.74 (d, 2H, J = 7.4, ArH), 8.73 (d, 2H, J = 8.0, ArH), 8.18 (br s, 2H, ArH), 8.00 (dd, 2H, J = 8.0 and 7.4, ArH), 7.52 (br s, 2H, ArH), 4.87 (br s, 4H, $2CH_2N$), 3.90 (t, 4H, J = 5.3, $2CH_2N$), 3.33 (t, 4H, J = 7.3, $2CH_2N$), 2.59 (m, 2H, CH_2). This compound was suspended in absolute EtOH, and methanesulfonic acid (0.04 mL, 0.60 mmol) was added. The corresponding dimethanesulfonate dihydrate (146 mg, 77%) was isolated by filtration and washed with diethyl ether: mp 151 °C dec; IR (KBr) 3410, 2750, 1690, 1645 cm^{-1}; ^{1}H NMR (DMSO-d_6) δ 8.90 (d, 2H, J = 7.9, ArH), 8.80 (br s, 2H, ArH), 8.58 (br s, 4H, $2NH_2^+$), 8.55 (m, 4H, ArH), 8.00 (m, 2H, ArH), 7.94 (m, 2H, ArH), 4.40 (t, 4H, J = 5.5, $2CH_2N$), 3.48 (br s, 4H, $2CH_2N$), 3.00 (br s, 4H, $2CH_2N$), 2.30 (s, 6H, $2CH_3$), 1.90 (m, 2H, CH_2); ^{13}C NMR (DMSO-d_6) δ 164.0, 163.9, 151.3, 150.5, 130.5, 129.1, 128.9, 127.4, 125.6, 124.7, 122.6, 118.7, 116.6, 107.1, 45.3, 44.3, 39.6, 36.5, 22.1; MS (ESI) *m*/*z* 601 ([M + H]$^+$). Anal. ($C_{35}H_{28}N_4O_6$·$2CH_3SO_3H$·$2H_2O$) C, H, N, S.

Absorption Spectra and Melting Temperature. Melting curves were measured using an Uvikon 943 spectrophotometer coupled to a Neslab RTE111 cryostat. For each series of measurements, 12 samples were placed in a thermostatically controlled cell holder, and the quartz cuvettes (10 mm path length) were heated by circulating water. Measurements were performed in BPE buffer (6 mM Na_2HPO_4, 2 mM

NaH_2PO_4, and 1 mM EDTA) at pH 7.1. The temperature inside the cuvette was measured with a platinum probe; it was increased over the range of 20−100 °C with a heating rate of 1 °C/min. The "melting" temperature (T_m) was taken to be the midpoint of the hyperchromic transition. The Uvikon 943 spectrophotometer was also used to record the absorption spectra.

Immobilization of DNA and Surface Plasmon Resonance. Two 5′-biotin-labeled DNA hairpins (PAGE-purified; Eurogentec) were used in surface plasmon resonance studies (hairpin loop underlined): d(biotin-CATATATATCCCCATATATATG) and d(biotin-CGCGCGCGTTTTCGCGCGCG). Samples of hairpin DNA oligomers in HBS-EP buffer at 25 nM were applied to flow cells in streptavidin-derivatized sensor chips (BIAcore SA chips) by direct flow at 2 μL/min in a four-channel BIAcore 3000 optical biosensor system. The sensor chips were conditioned with four consecutive 1 min injections of 1 M NaCl in 50 mM NaOH and three consecutive 15 s injections of 0.1% SDS in 3.5 mM EDTA, followed by extensive washing with buffer. Nearly the same amounts of all oligomers were immobilized on the surface by noncovalent capture, leaving one of the flow cells blank as a control. Manual injection was used with a flow rate of 2 μL/min to achieve long contact times with the surface and to control the amount of DNA bound to the surface. All procedures for binding studies were automated as methods using repetitive cycles of sample injection and regeneration. Steady-state binding analysis was performed with multiple injections of different compound concentrations over the immobilized DNA surfaces for a 15 min period at a flow rate of 20 μL/min and 25 °C. Drug solutions with known concentrations from 1.5 nM to 1.5 μM were prepared in filtered and degassed buffer by serial dilutions from a stock solution and were injected from 7 mm plastic vials with pierceable plastic crimp caps (BIAcore Inc.). In all cases, the DNA surface was regenerated by buffer flow over the course of 30 min without additional regeneration agents.

The instrument response (RU) in the steady-state region is proportional to the amount of bound drug and was determined by linear averaging over a 80 s time span. The predicted maximum response per bound compound in the steady-state region (RU_{max}) is determined from the DNA molecular weight, the amount of DNA in the flow cell, the compound molecular weight, and the refractive index gradient ratio of the compound and DNA (*36*, *37*). In the present case, the observed RU values at high concentrations are greater than RU_{max}, pointing to several binding sites in these DNA sequences. The number of binding sites was determined from Scatchard plots derived from plots of RU/concentration versus RU using linear regression analysis (data not shown). The RU_{max} value is required to convert the observed response (RU) to the standard binding parameter r (moles of drug bound per mole of DNA hairpin) using the equation

$$r = \mathrm{RU}/\mathrm{RU}_{max}$$

Average fitting of the sensorgrams at the steady-state level was performed with the BIAevaluation 3.0 program. To obtain the affinity constants, the results from the steady-state region were fitted with a multiple-equivalent site model using Kaleidagraph for nonlinear least-squares optimization of the binding parameters with the following equation:

$$r = (nKC_{free})/(1 + KC_{free})$$

where K, the microscopic binding constant, is one variable to fit, r represents the moles of bound compound per mole of DNA hairpin duplex (*38*), C_{free} is the concentration of the compound in equilibrium with the complex and is fixed by the concentration in the flow solution, and n is the number of compound binding sites on the DNA duplex and is the second variable to fit. The r values are calculated by the ratio RU/RU_{max}, where RU is the steady-state response at each concentration and RU_{max} is the predicted RU for binding of a single compound to the DNA in a flow cell. Global kinetic fits to the sensorgrams to obtain association and dissociation kinetic constants were done using BIAevaluation software and an equivalent site interaction model.

Electric Linear Dichroism. ELD measurements were performed with a computerized optical measurement system using the procedures previously outlined (*39*, *40*). All experiments were conducted with a 10 mm path length Kerr cell having an electrode separation of 1.5 mm. The samples were oriented under an electric field strength varying from 1 to 14 kV/cm. The drug being tested was present at 10 μM together with the DNA at 200 μM unless otherwise stated. This electro-optical method has proved to be most useful in determining the orientation of the drugs bound to DNA. It has the additional advantage that it senses only the orientation of the polymer-bound ligand: the free ligand is isotropic and does not contribute to the signal (*41*).

DNA Relaxation Experiments. Supercoiled pKMp27 DNA (0.4 μg) was incubated with 4 units of human topoisomerase I or II (TopoGen Inc.) at 37 °C for 1 h in relaxation buffer [50 mM Tris (pH 7.8), 50 mM KCl, 10 mM $MgCl_2$, 1 mM dithiothreitol, and 1 mM EDTA] in the presence of varying concentrations of the drug under study. Reactions were terminated by adding SDS to a concentration of 0.25% and proteinase K to 250 μg/mL. DNA samples were then added to the electrophoresis dye mixture (3 μL) and electrophoresed in a 1% agarose gel at room temperature for 2 h at 120 V. Gels were stained with ethidium bromide (1 μg/mL), washed, and photographed under UV light. Similar experiments were performed using ethidium-containing agarose gels (*42*).

DNase I Footprinting. The 117 and 265 bp DNA fragments were prepared by 3′-^{32}P end labeling of the *Eco*RI−*Pvu*II double digest of the pBS plasmid (Stratagene) using [α-^{32}P]dATP (Amersham, 3000 Ci/mmol) and AMV reverse transcriptase (Roche). The two 198 bp fragments were obtained from plasmids pMS1 and pMS2 (kindly provided by K. R. Fox, University of Southampton, Southampton, U.K.) after digestion with the restriction enzymes *Hin*dIII and *Xba*I (*43*). In each case, the labeled digestion products were separated on a 6% polyacrylamide gel under nondenaturing conditions in TBE[1] buffer [89 mM Tris-borate (pH 8.3) and 1 mM EDTA]. After autoradiography, the requisite band of DNA was excised, crushed, and soaked in water overnight at 37 °C. This suspension was filtered through a Millipore 0.22 μm filter, and the DNA was precipitated with ethanol. After washing with 70% ethanol and vacuum drying of the precipitate had been carried out, the labeled DNA was resuspended in 10 mM Tris (adjusted to pH 7.0) containing 10 mM NaCl.

[1] Abbreviation: TBE, Tris-borate-EDTA.

Bovine pancreatic deoxyribonuclease I (DNase I, Sigma Chemical Co.) was stored as a 7200 units/mL solution in 20 mM NaCl, 2 mM $MgCl_2$, and 2 mM $MnCl_2$ (pH 8.0). The stock solution of DNase I was kept at −20 °C and freshly diluted to the desired concentration immediately prior to use. Footprinting experiments were performed essentially as previously described (*44*). Briefly, reactions were conducted in a total volume of 10 μL. Samples (3 μL) of the labeled DNA fragments were incubated with 5 μL of the buffered solution containing the ligand at appropriate concentration. After incubation for 30 min at 37 °C to ensure equilibration of the binding reaction, the digestion was initiated by the addition of 2 μL of a DNase I solution whose concentration was adjusted to yield a final enzyme concentration of ∼0.01 unit/mL in the reaction mixture. After 3 min, the reaction was stopped by freeze-drying. Samples were lyophilized and resuspended in 5 μL of an 80% formamide solution containing tracking dyes. The DNA samples were then heated at 90 °C for 4 min and chilled in ice for 4 min prior to electrophoresis.

DNA cleavage products were resolved by polyacrylamide gel electrophoresis under denaturing conditions (0.3 mm thick, 8% acrylamide containing 8 M urea). After electrophoresis (∼2.5 h at 60 W and 1600 V in a Tris-Borate-EDTA-buffered solution), gels were soaked in 10% acetic acid for 10 min, transferred to Whatman 3MM paper, and dried under vacuum at 80 °C. A Molecular Dynamics 425E PhosphorImager was used to collect data from the storage screens exposed to dried gels overnight at room temperature. Baseline-corrected scans were analyzed by integrating all the densities between two selected boundaries using ImageQuant version 3.3. Each resolved band was assigned to a particular bond within the DNA fragments by comparison of its position relative to sequencing standards generated by treatment of the DNA with dimethyl sulfate followed by piperidine-induced cleavage at the modified guanine bases in DNA (G-track).

Cell Cultures and Survival Assay. Human CEM leukemia cells were obtained from the American Tissue Culture Collection. Cells were grown at 37 °C in a humidified atmosphere containing 5% CO_2 in RPMI 1640 medium, supplemented with 10% fetal bovine serum, L-glutamine (2 mM), 1.5 g/L sodium bicarbonate, 4.5 g/L glucose, 10 mM HEPES, 1 mM sodium pyruvate, penicillin (100 IU/mL), and streptomycin (100 μg/mL). The cytotoxicity of the test compounds was assessed using a cell proliferation assay developed by Promega (CellTiter 96 AQ_{ueous} one solution cell proliferation assay). Briefly, 3×10^4 exponentially growing cells were seeded in 96-well microculture plates with various drug concentrations in a volume of 100 μL. After incubation for 72 h at 37 °C, 20 μL of the tetrazolium dye was added to each well and the samples were incubated for a further 2 h at 37 °C. Plates were analyzed on a Labsystems Multiskan MS (type 352) reader at 492 nm.

Cell Cycle Analysis. For flow cytometric analysis of DNA content, 10^6 cells in exponential growth phase were treated with graded concentrations of the test drug for 24 h and then washed three times with citrate buffer. The cell pellet was incubated with 250 μL of trypsin-containing citrate buffer for 10 min at room temperature and then with 200 μL of citrate buffer containing a trypsin inhibitor and RNase (10 min) prior to adding 200 μL of propidium iodide (PI) at 125 μg/mL. Samples were analyzed on a Becton Dickinson FACScan flow cytometer using the LYSYS II software which is also used to determine the percentage of cells in the different phases of the cell cycle. PI was excited at 488 nm, and the fluorescence was analyzed at 620 nm on channel Fl-3.

Bromodeoxyuridine (BrdU) Incorporation. Cells were cultured in complete RPMI 1640 medium with the test drug at different concentrations for 24 h prior to harvesting and then pulse labeled with 10 μM BrdU for 60 min in complete medium. Following two washes in phosphate-buffered saline (pH 7.3) with 0.1% sodium azide, cells were fixed in 70% ethanol and incubated for 1 h at 4 °C. Following another wash in phosphate-buffered saline, cells were denatured in 2 N HCl for 15 min at 37 °C (or for 30 min at room temperature) under gentle stirring. The pH was adjusted by a short incubation (5 min) in 3 mL of 0.1 M $Na_2B_4O_7$ (pH 8.5) before centrifugation (5 min at 500*g* and 4 °C). The cell pellet was then washed with 5 mL of buffer containing PBS, Tween 0.05%, and 0.1% BSA (bovine serum albumin fraction V), resuspended in 50 μL of this buffer, and then incubated with the fluorescein isothiocyanate (FITC)-conjugated anti-BrdU monoclonal antibody (Becton Dickinson, San Jose, CA) for 30 min at room temperature in the dark. For the negative controls, the pellet was incubated without antibody. All cell pellets were washed with 1 mL of buffer containing PBS, Tween 0.05%, and 0.1% BSA. Cells were collected by centrifugation and counterstained with 10 μg/mL propidium iodide and treated with RNase (1 μg/mL). Samples were analyzed on a Becton Dickinson FACScan flow cytometer using the LYSYS II software.

Confocal Microscopy. The cells (7×10^5 cells/mL) were incubated at 37 °C with the test compound at 10 or 20 μM for 4 h. The medium was removed, and cells were rinsed with ice-cold PBS (10 min) prior to the fixation with a 2% paraformaldehyde solution for 20 min at 4 °C. After being washed, the cells were incubated with the fluorescent probe $DiOC_6$ (150 nM, 3,3-dihexyloxacarbocyanine iodide, Molecular Probes Inc.) for 5 min at 37 °C in the dark, washed again twice with PBS, and then incubated with a solution of propidium iodide (0.5 μg/mL) for 5 min at room temperature. A drop of anti-fade solution was added, and the treated portion of the slide was covered with a glass coverslip. The fluorescence of the drugs was detected by confocal microscopy using a Leica DMIRBE microscope controlled by a Leica TCS-NT workstation (Leica Microsystems, Bensheim, Germany) with a 63 × 1.32 NA oil objective, equipped with 75 mW argon−krypton and Coherent Innova-90-UV laser lines. The emission signal was observed through a dichroic mirror (DD488/568) followed by a filter set (RSP 580, BF 530/30, BP 600/30, and BP460/30 for UV-excited probes). The optical sections were obtained in the *Z*-axis and stored on the computer with a scanning mode. In all cases, the operating conditions were such that detectable images could not be obtained for cell samples not treated with drugs.

RESULTS

Absorption spectral titrations for **MCI3334** and **MCI3335** reveal quite significant differences in behavior (Figure S1). There is a large hypochromism (56%) and a clear isosbestic point at 403 nm with the DNA complexes of the monomeric

Table 1: Binding Constants and Kinetic Parameter for Drug Binding to DNA[a]

compound	sequence	K_{eq} (M^{-1})	k_a (M^{-1} s^{-1})	k_d (s^{-1})	k_a/k_d (M^{-1})	*n*
MCI3334	$[AT]_4$	4.6×10^4	80.9	1.3×10^{-2}	6.31×10^3	8−10
	$[CG]_4$	1.38×10^5	4.33×10^3	1.1×10^{-2}	3.83×10^5	3−4
MCI3335	$[AT]_4$	1.44×10^7	—[b]	—[b]	—[b]	5
	$[CG]_4$	1.83×10^8	2.12×10^5	1.45×10^{-3}	1.46×10^8	1−2

[a] Experiments were performed in HBS-EP buffer at 25 °C. The DNA sequences show one strand of the duplex stem of the hairpin used in the BIAcore SPR experiments. The number of compound binding sites on the DNA duplexes is indicated (*n*). [b] Not indicated, fitting not satisfactory.

compound, whereas the extent of hypochromism is lower (34%) with the dimeric analogue. However, at low DNA concentrations, the decrease in the absorbance peak at 377 nm is more pronounced with the dimer than with the monomer and the bathochromic shift is larger (7 and 4 nm for the dimer and monomer, respectively). The lack of isosbestic points with **MCI3335** when titrated with a DNA solution can be explained by the existence of two binding modes (mono- and bis-intercalation for example), and/or by a stronger tendency of the dimeric compound than of the monomer to self-associate. Stacking interactions are frequently observed with planar aromatic drug molecules (*45*), and one might intuitively expect stronger stacking interaction with a dimeric compound than with a monomeric molecule. To support this idea, we recorded the absorption and fluorescence spectra of the drugs in the absence and presence of the detergent sodium dodecyl sulfate (SDS). Addition of 1% SDS to a solution of **MCI3334** and **MCI3335** induces significant perturbation of their absorption and fluorescence spectra (Figure S2). The spectral changes induced by SDS are particularly important for the dimer, with significant hypsochromic and hyperchromic effects and a 6-fold increase in the fluorescence intensity compared to that in the SDS-free drug solution. Stacking interactions likely occur in both cases, but they are much more pronounced for the dimer than for the monomer.

The interaction of the two drugs with calf thymus DNA was also investigated by thermal denaturation analysis. Plots of the relative absorbance change at 260 nm versus temperature (Figure S3) show that the dimer stabilizes the double-helix structure of DNA much more strongly than the monomer. ΔT_m ($T_m^{drug-DNAcomplex} - T_m^{DNAalone}$) values of 6.5 and 24.3 °C were measured with **MCI3334** and **MCI3335**, respectively, for a drug:DNA phosphate ratio of 0.1. The high thermal stability of DNA observed in the presence of **MCI3335** provided the first indication that both moieties of this dimer participate in the DNA binding reaction.

Surface plasmon resonance (SPR) was used to evaluate more accurately the strength of the interaction of the drugs with specific DNA sequences. The biosensor analysis was performed with the monomeric and dimeric compounds, both water soluble, using a streptavidin-coated sensor chip (SA) and two hairpin oligomers containing an $[AT]_4$ or a $[CG]_4$ tract.

A set of SPR sensorgrams at different concentrations of **MCI3334** and **MCI3335** binding to both DNA sequences is shown in Figure 2. As can be seen, the monomeric compound binds poorly to both the AT and CG sequences. The interaction is considerably weaker than that to the dimer which shows well-resolved binding to the DNA sequences in a concentration-dependent way. There are also considerable differences between the two compounds in terms of kinetics. The dissociation of **MCI3334** from DNA is extremely rapid, whereas slow dissociation kinetics are observed with **MCI3335**. However, in both cases, the dissociation of the drug−DNA complexes was achieved by injection of a buffer solution, without detergent.

The steady-state SPR binding results allow us to determine and compare DNA binding affinities as well as the stoichiometry of the interaction. SPR data were analyzed by plotting *r* versus drug concentration and fitting the binding results as described in Materials and Methods to determine the macroscopic binding constants and stoichiometries. The best fit of the binding results gave the K_{eq} values listed in Table 1. With the monomer, the binding constant for the AT sequence is 3 times lower than for the CG sequence. The difference is more pronounced for the dimer, with a K_{eq}^{CG}/K_{eq}^{AT} ratio of 12. This reflects a clear preference for CG over AT sites, in agreement with the footprinting experiments (see below). The affinity of the dimer for DNA is extremely high, in the 10^7-10^8 M^{-1} range, what corresponds to a 1000-fold increase compared to that of the monomer. There is no doubt that the two moieties of the dimer contribute to the DNA binding process.

As expected for intercalating drugs, the predicted maximum response per bound compound in the steady-state region (RU_{max}) is in all cases lower than the RU values obtained at high drug concentrations. This points to the existence of several binding sites in these DNA sequences.

Considering the length of the hairpin oligonucleotides and the size of the drug molecules, we can estimate that each DNA can offer approximately three or four drug intercalation binding sites for the monomer and probably not more than two for the dimer. This prediction is consistent with the experimental observations for the drugs interacting with the $[CG]_4$ sequence. With the $[AT]_4$ sequence, higher *n* values were calculated (>4), and this must reflect the existence of a secondary binding mode, probably an external electrostatic interaction as has been observed with other cationic DNA ligands (*46*). The fitting of the SPR data for MCI3335 bound to the $[AT]_4$ sequence with a one-site model is not ideal (Figure S4), but a two-site model did not give a better result. The unusual shape of the AT sensorgrams must reflect a complicated binding process, which we have not yet properly dissected. However, it is essential to note that with both AT and CG sequences, the number of binding sites determined with the monomer is about twice that calculated with the dimer. This is again another indication suggesting that the two halves of the bidentate molecule are engaged in the DNA recognition process.

The analysis of the kinetic parameters also revealed large differences between the two drugs. Visual inspection of the binding sensorgrams in Figure 2 is sufficient to conclude that the dimer exhibits much slower dissociation rates in both

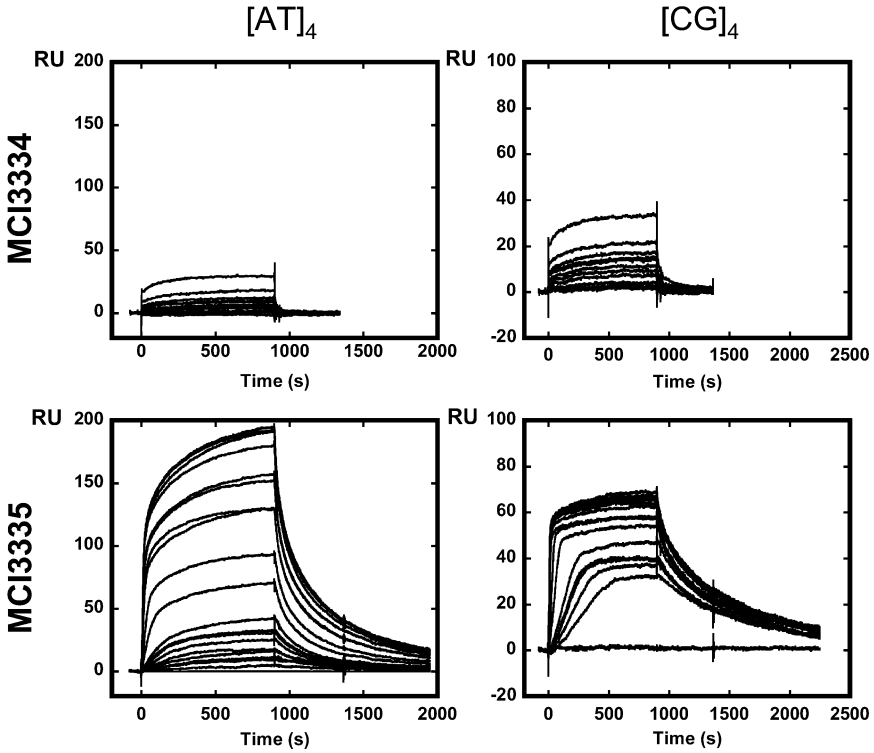

FIGURE 2: SPR sensorgrams for binding of **MCI3334** and **MCI3335** to the $[AT]_4$ and $[CG]_4$ DNA hairpin oligomers in HBS-EP buffer at 25 °C. The concentration of the unbound ligand in the flow solution varies from 1 nM in the bottom curve to 2.5 μM in the top curve.

the AT and GC interactions than the monomer. A global equivalent site model was used to fit the experimental SPR curves and provided satisfactory results (with very small residuals, data not shown). We were able to calculate the association and dissociation kinetic constants (Table 1), except for the dimer interacting with the AT sequence which gave a nonsatisfactory fitting regardless of the binding model that was used. Due to the lack of confidence in the calculated k_a and k_d values with the dimer−AT complex, we decided not to take them into account. The dissociation of the monomer from the $[CG]_4$ sequence is more than 1 order of magnitude faster than that of the dimer. The difference is more pronounced at the association level. With the GC sequence, the $k_a^{dimer}/k_a^{monomer}$ ratio amounts to 50 which reflects a significant gain of stability for the DNA complexes with the bidentate molecule, and this probably accounts for the stronger footprints seen with the dimer compared to the monomer. The binding constants determined by the k_a/k_d ratio are relatively close to the values determined using the steady-state fitting method, at least for the GC oligonucleotide. The K_{eq} and k_a/k_d values concur that the dimeric molecule exhibits an extremely high affinity for the $[CG]_4$ sequence.

Electric linear dichroism (ELD) is an electro-optical method well suited to defining the orientation of small molecules bound to nucleic acids (*41*). Here we have exploited this spectroscopic technique by employing a polarized light to define more precisely the binding process for **MCI3334** and **MCI3335**. The measurements were performed in a low-ionic strength buffer [1 mM sodium cacodylate buffer (pH 7.0)] because of the high electric field applied to the DNA samples (up to 14 kV/cm). The ELD spectra of **MCI3334** and **MCI3335** bound to calf thymus DNA show negative reduced dichroism ($\Delta A/A$) values in the drug absorption band (Figure 3a). In both cases, the 300−450 nm negative band reflects the orientation of the furonaphthalimide chromophore along the electric field. The variations in $\Delta A/A$ with the electric field strength were recorded at a DNA:drug ratio of 20 when the drug molecules are fully bound to DNA (Figure 3b). The fact that $\Delta A/A$ depends similarly upon the field strength for the drug−DNA complexes at 380 nm and the DNA bases at 260 nm in the absence of ligand (Figure 3c) indicates that in both cases the drug chromophores are oriented perpendicular to the electric field as expected for an intercalative binding. The binding of the drugs to DNA likely induces a stiffening effect, explaining the higher reduced dichroism value measured in the absorption band of the drugs than in the DNA absorption band. Similar ELD data were obtained with the synthetic polynucleotides $poly(dAT)_2$ and $poly(dGC)_2$ (data not shown). These spectroscopic measurements strongly suggest that the two drugs intercalate into DNA, but mono- and bis-intercalation cannot be differentiated by the ELD method.

We tried to use a DNA unwinding assay based on the relaxation of supercoiled plasmid DNA in the presence of topoisomerase I to distinguish mono- versus bis-intercalation. Supercoiled DNA was treated with topoisomerase I in the presence of increasing concentrations of the test drugs. The DNA relaxation products were then resolved by agarose gel electrophoresis (Figure S5). Both **MCI3334** and **MCI3335** affect the relaxation of DNA by topoisomerase I. Here again, the effect is more pronounced with the dimer than with the monomer. The gel shift induced by the dimer (due to strong binding) perturbs the electrophoretic migration of the DNA species, and therefore, a direct comparison is difficult. The two compounds unwind closed circular duplex DNA, but a quantitative estimation of the unwinding angle is not possible by this method. Nevertheless, this topoisomerization assay

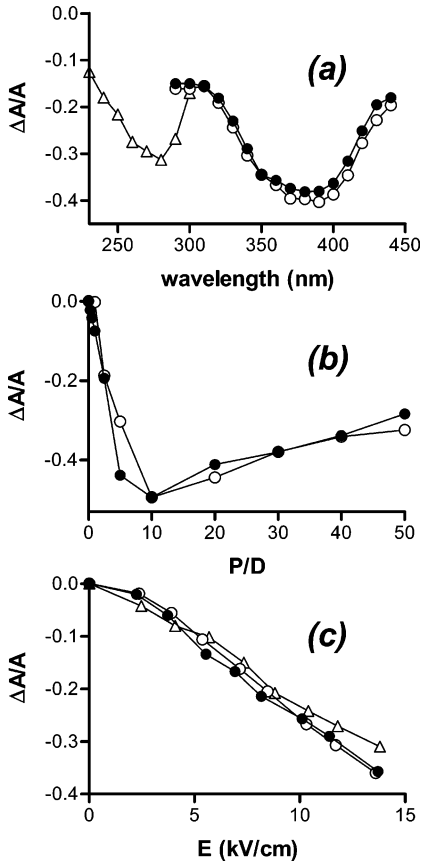

FIGURE 3: Dependence of the reduced dichroism $\Delta A/A$ on (a) the wavelength, (b) the DNA phosphate:drug ratio (P:D), and (c) the electric field strength: (●) **MCI3334**, (○) **MCI3335**, and (△) DNA alone. The conditions were as follows: (a) 13.6 kV/cm and P/D = 20 (200 μM DNA and 10 μM drug), (b) 380 nm and 13.6 kV/cm, and (c) 380 nm and P/D = 20 for the DNA−drug complexes and 260 nm for the DNA alone, in 1 mM sodium cacodylate buffer (pH 7.0).

shows once again that the dimer binds tightly to both the supercoiled and nicked DNA forms of the plasmid, as indicated by the important shift of these two DNA bands (Figure S4).

It is important to mention at this point that the two compounds affect topoisomerase I activity via DNA intercalation but they do not inhibit the catalytic activity of the enzyme. The drugs do not promote DNA cleavage by topoisomerase I or II, in contrast to the reference inhibitors camptothecin and etoposide (Figure S4). The intensity of the band corresponding to nicked DNA (for topoisomerase I) and linear DNA (for topoisomerase II) is not amplified in the presence of these naphthalimide derivatives. Neither **MCI3334** nor **MCI3335** stabilizes DNA−topoisomerase II covalent complexes.

The DNase I footprinting methodology was employed to compare the sequence selectivity of the monomeric and dimeric naphthalimide compounds. Four DNA restriction fragments were prepared by 3′-end radiolabeling with ^{32}P. On one hand, we used a 117 bp and a 265 bp DNA fragment from plasmid pBS with random DNA sequences. These two pieces of DNA have been used previously to study sequence recognition by amonafide and elinafide (*14*), and therefore, the binding sites can be compared. On the other hand, we prepared two designed fragments of 198 bp termed "universal footprinting substrates" (*43*) containing all 136 distinguishable tetranucleotide sequences [$(4^4)/2 + (4^{4/2})/2 = 136$]. These two fragments, MS1 and MS2, contain the same sequence of 136 bp but cloned in the opposite orientation (5′ → 3′ and 3′ → 5′, respectively). With each fragment, the products of digestion by DNase I in the absence and presence of the test drugs were resolved by polyacrylamide gel electrophoresis. Typical DNase I digestion patterns observed in the absence and presence of the test compounds are illustrated in Figure 4. Significant differences between the dimeric compound and the monomeric analogues can easily be seen. Intense footprints are detected with **MCI3335**, whereas the effects are much less pronounced with **MCI3334**. However, the monomer does alter the DNase I cleavage profiles and appears to bind to the same type of sequences as the dimer, but with a reduced affinity. A typical example can be seen with the MS1 fragment where a solid footprint develops around nucleotide position 60 with the dimer and to a lower extent with the monomer. This well-resolved binding site corresponds to a GC-rich sequence. The difference between the two drugs is also clearly visible with the 265-mer (Figure 4C). In this case, the monomer modestly inhibits DNase I cleavage whereas the dimer produces several footprints separated by regions where the DNase I cleavage is strongly enhanced. These regions where there is more cutting by the enzyme are commonly attributed to drug-induced structural changes in the vicinity of the binding sites, as a result of the intercalative process (*47*). A densitometric analysis of the different patterns was performed to estimate the location and relative strength of binding at particular DNA sites. Figure 5 shows the differential cleavage plots for the four DNA fragments in the presence of the two compounds. The dips in these plots (negative values) indicate sites of protection from DNase I cleavage, whereas peaks (positive values) indicate regions of drug-induced enhancement of nuclease cleavage. All binding sites identified for the dimer coincide with the position of GC-rich sequences. AT-rich sequences, in particular, runs of consecutive A and T bases, are excluded from the binding sites and often appear in regions of enhanced cleavage by DNase I. The most intense footprints are detected at GC sites. The sequence mentioned above around position 60 on fragment MS1, 5′-CGTCCGGTGGG, provides a strong receptor for the dimeric molecule. Similarly, the sequences 5′-CCAGG and 5′-CGGGA on fragment MS2 show full protection with **MCI3335** only. Several other similar sequences (5′-GCGG, 5′-AGCC, 5′-GGGCG, 5′-CGCC, and 5′-CGGCCAG) are identified as preferential binding sequences.

A tetrazolium-based assay was applied to determine the drug concentration required to inhibit the growth of CEM human leukemia cells by 50% after incubation in the culture medium for 72 h (Figure 6). The dimer proved to be considerably, more than 100 times, more cytotoxic than the monomer, with IC_{50} values of 0.6 μM and 4.9 nM determined for **MCI3334** and **MCI3335**, respectively. Flow cytometric analysis of propidium iodide-labeled CEM cells revealed that **MCI3334** induces a slight accumulation of cells in the G2/M phase which is concomitant with a decrease of the G0/G1 cell population. The percentage of cells in the S phase increases from 32 to 40% (Figure 7). The dimer **MCI3335** showed little effect on cell cycle progression. In fact, this compound binds so tightly to DNA that a dose-dependent decrease in the level of the PI labeling occurs, as illustrated

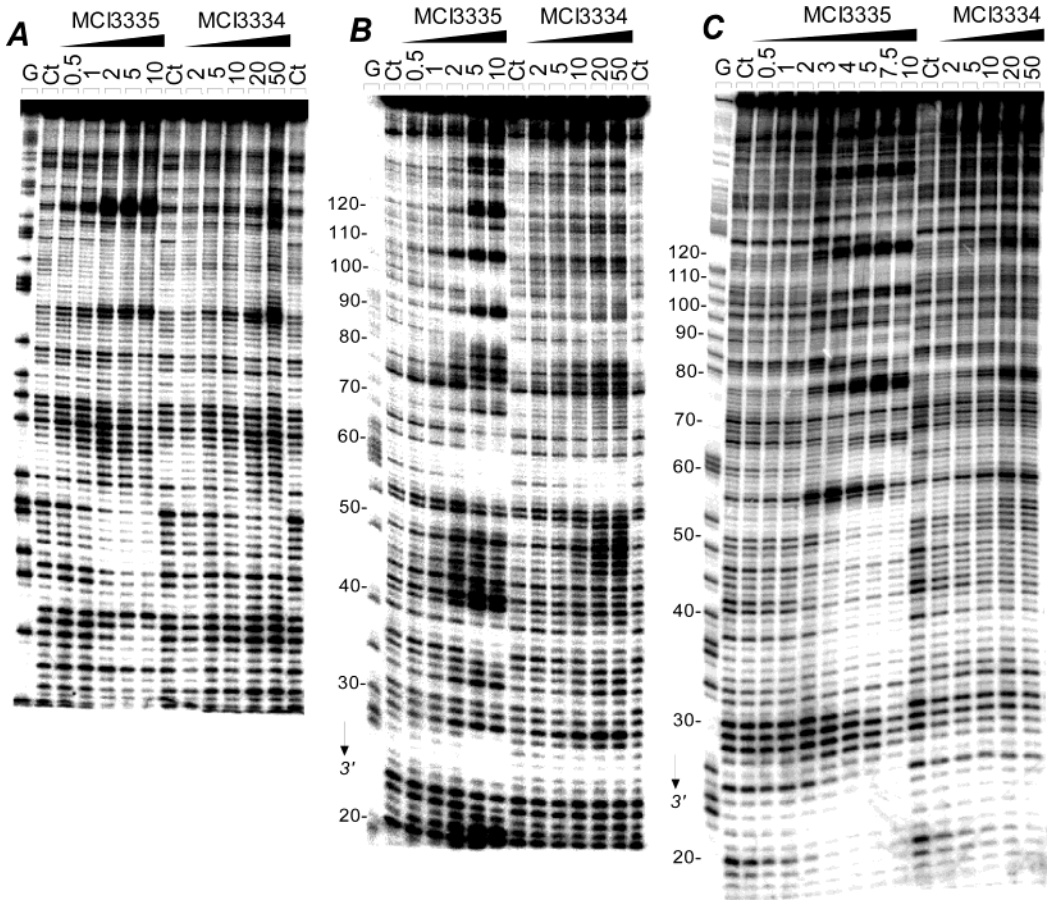

FIGURE 4: Sequence selective binding of **MCI3334** and **MCI3335**. The gels show DNase I footprinting with three DNA restriction fragments of (A) 117, (B) 198, and (C) 265 bp. The 117-mer and 265-mer *Pvu*II−*Eco*RI fragments were cut from the plasmid pBS. The 198-mer *Hin*dIII−*Xba*I fragment was obtained from plasmid pMS1. In each case, the DNA was 3′-end labeled at the *Eco*RI or *Hin*dIII site with [α-^{32}P]dATP in the presence of AMV reverse transcriptase. The products of nuclease digestion were resolved on an 8% polyacrylamide gel containing 7 M urea. Control tracks (marked Ct) contained no drug. Guanine-specific sequence markers obtained by treatment of the DNA with dimethyl sulfate followed by piperidine were run in the lanes marked G. Numbers on the side of the gels refer to the standard numbering scheme for the nucleotide sequence of the DNA fragment.

in Figure 7. To obtain a more precise view of the drug effect at the S phase level, cells were labeled with bromodeoxyuridine (BrdU), a thymidine analogue which is incorporated into newly synthesized strands of DNA. As shown in Figure 8, many fewer BrdU$^+$ cells, labeled in the S phase at the time of treatment, were detected after incubation for 24 h with **MCI3335** than with **MCI3334** compared to the control cell population. The dimer is significantly more potent than the monomer at inhibiting the incorporation of BrdU into DNA. The enhanced DNA binding capacity of **MCI3335** likely accounts for the potent inhibition of DNA synthesis which is probably at the origin of the increased cytotoxicity of this dimeric molecule.

Finally, we studied the intracellular distribution of the compounds in the CEM cells by means of confocal microscopy, taking advantage of the intrinsic fluorescence of the furonaphthalimide nucleus (Figure 9). In recent studies, we have shown that this approach is very useful in distinguishing the nuclear versus cytoplasmic distribution of DNA-targeted drugs (*48*−*50*). The cells were treated with the monomer or dimer compound at 5, 10, or 20 μM for 4 h at 37 °C, washed, fixed with 2% paraformaldehyde, and then counterstained with the green fluorescent dye 3,3-dihexyloxacarbocyanine iodide (150 nM $DiOC_6$), and/or with the red fluorescent dye propidium iodide (0.5 μg/mL). PI is routinely used to stain cell nuclei and to label DNA in cytometry studies, whereas $DiOC_6$ which binds selectively to mitochondria (possibly to reticulum also) was used here to stain the cytoplasm of CEM cells in green. The three colors, blue, green, and red, can be easily differentiated by confocal microscopy. The high-resolution fluorescence pictures presented in Figure 9 show that the monomer **MCI3334** selectively accumulates in the cell nuclei whereas with the dimer **MCI3335** (which is less fluorescent than the monomer), the blue fluorescence is more uniformly distributed in both the cytoplasm and the nucleus of the cells. The marked purple fluorescence seen in the cells doubly stained with **MCI3334** and PI suggests that a significant proportion of the drug molecule must be bound to genomic DNA. In contrast, the **MCI3335** blue signal clearly colocalizes with both the $DiOC_6$ green signal and the PI red signal. The dimer shows a reduced nuclear uptake capacity compared to the monomer, but a massive nuclear accumulation in the cell nuclei is not absolutely required for the dimer to exert its high cytotoxicity.

DISCUSSION

The monomer **MCI3334** and the dimer **MCI3335** are characterized by a furan ring fused to the naphthalene moiety. This additional heterocycle distinguishes **MCI3335** from elinafide, the rest of the molecule being identical, in

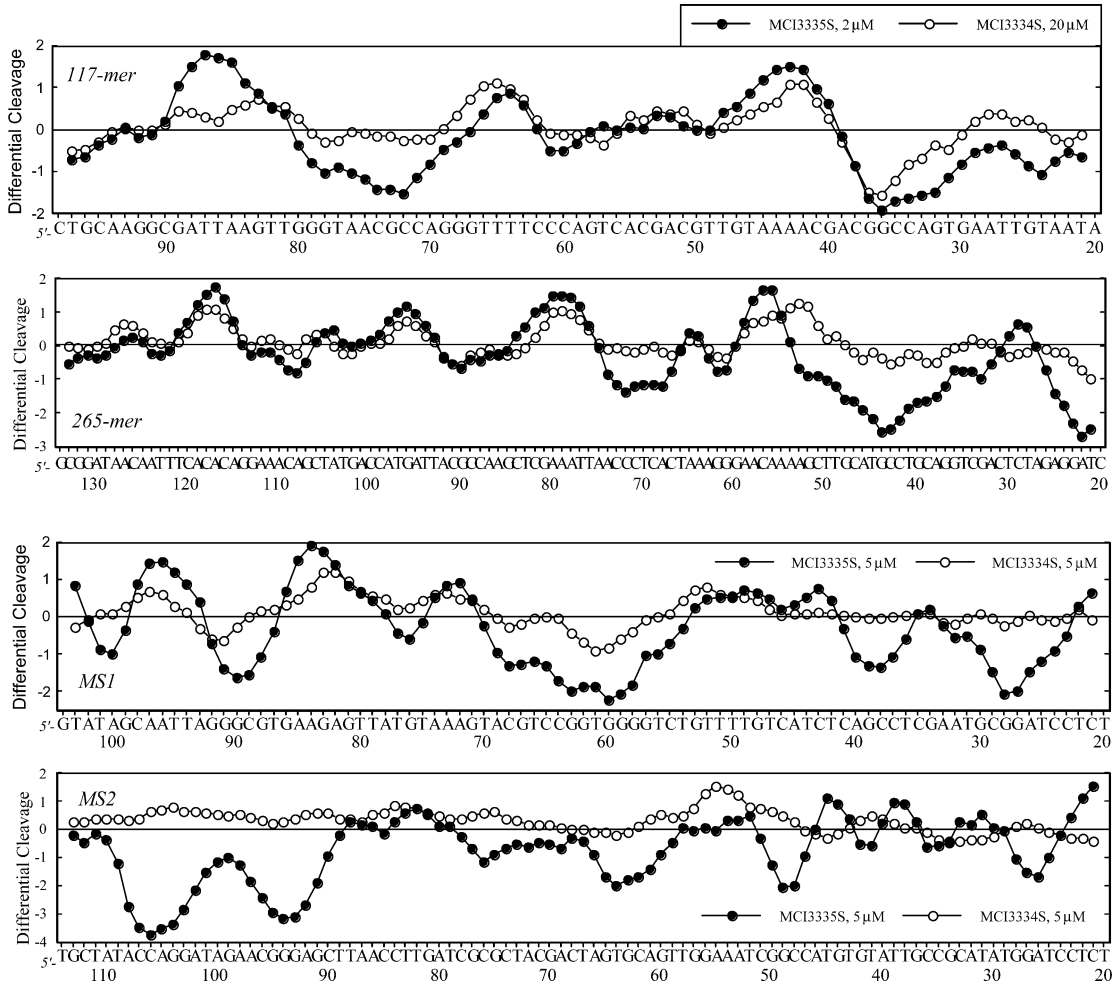

FIGURE 5: Differential cleavage plots comparing the susceptibility of the different DNA fragments to DNase I cutting in the presence of **MCI3334** and **MCI3335** at the indicated concentrations. Negative values correspond to a ligand-protected site, and positive values represent enhanced cleavage. Vertical scales are in units of $\ln(f_a) - \ln(f_c)$, where f_a is the fractional cleavage at any bond in the presence of the drug and f_c is the fractional cleavage of the same bond in the control, given closely similar extents of overall digestion. Each line represents a three-bond running average of individual data points, calculated by averaging the value of $\ln(f_a) - \ln(f_c)$ at any bond with those of its two nearest neighbors. Only the region of the restriction fragments analyzed by densitometry is shown.

particular, the nature of the aminoalkyl linker between the two planar units. The range of biochemical and biophysical data reported here demonstrates that the dimerization of the furonaphthalimide system considerably reinforces the capacity of the drug to bind to DNA. A qualitative analysis of the DNA binding reaction by means of absorption and melting temperature measurements provided the first indications that binding strength was markedly enhanced for the dimer compared to that for the monomer. A full quantitative analysis, by means of the surface plasmon resonance technology, gave more precise information, revealing that the affinity of the dimer for DNA is ~1000 times higher than that of the monomer (K_{eq} in the 10^7-10^8 and 10^4-10^5 M^{-1} ranges for **MCI3335** and **MCI3334**, respectively). The use of this sophisticated technique to study DNA interaction with small molecules is highly valuable, at least for water soluble molecules, not only for measuring accurate binding constants but also for estimating the kinetic parameters of the interaction (*51*). The method has been extensively exploited by Wilson and co-workers in the study of extended small molecules that fit into the minor groove of DNA and RNA (*37*, *52*), and more recently, we started applying it to mono-intercalating drugs (*53*, *54*). SPR has been previously employed to study two types of bis-intercalating drugs, sandramycin (*55*) and ditercalinium (*56*), but this is the first case in which the technique is fully developed to compare a pair of monomeric and dimeric molecules. The monomer **MCI3334** displays considerably faster association rates than the dimer at both the $[AT]_4$ and $[CG]_4$ sequences. The k_d values are also quite distinct for the monomer and dimer. The rate of dissociation of **MCI3335** from the $[CG]_4$ sequence is ~7 times slower than that of **MCI3334**. The dimer, which exhibits a significant degree of self-stacking in aqueous solution, forms long-lived DNA complexes, and this effect no doubt accounts for the intense footprints detected with this compound.

The SPR data concur with the footprinting experiments to indicate that the dimeric compound presents a pronounced selectivity for GC-containing sequences. Although binding to AT sequences is far from negligible, the complexes formed at GC sites dissociate more slowly and the longer residence time must facilitate inhibition of DNA cleavage by the endonuclease. Interestingly, the sequence selectivity of **MCI3335** is not identical to that of elinafide. A comparison of the footprinting data presented here with those reported a few years ago with elinafide reveals that the newly designed

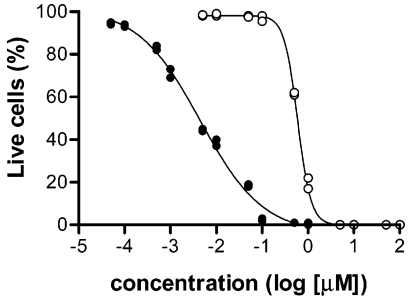

FIGURE 6: Cell growth inhibition curves. CEM leukemia cells were treated with the indicated concentrations of **MI3334** or **MCI3335**. Cell survival was assessed by a MTS assay after continuous drug exposure for 72 h.

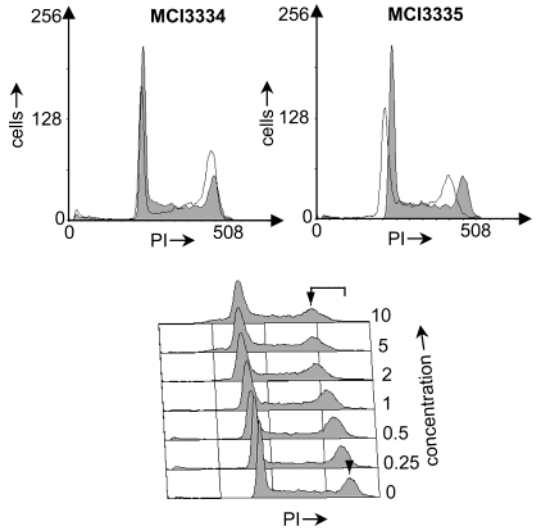

FIGURE 7: Cell cycle analysis of CEM human leukemia cells treated for 24 h with (top) 2 μM **MCI3334** or **MCI3335** and (bottom) increasing concentrations of **MCI3335**. Cells were analyzed with the FACScan flow cytometer.

furonaphthalimide dimer exhibits an enhanced selectivity toward GC sites compared to the parent compound. With the bis-tricyclic compound, a preference for mixed nucleotide sequences characterized by an alternating purine-pyrimidine motif, particularly those containing GpT (ApC) and TpG (CpA) steps, was deduced (*14*). In this case, the bis-tetracyclic molecule exhibits a different behavior with a marked preference for GC sites. The footprinting patterns produced by **MCI3335** rather resemble those obtained with acridine 4-carboxamide derivatives (*57*) and more recently with bis-dihydrodipyridopyrazines incorporating aminoalkyl linkers similar to that of **MCI3335** (*58*). The different behavior of elinafide and **MCI3335** suggests that the furano ring of the bis-tetracyclic dimer plays a part in determining GC selectivity. It seems that the origin of the sequence selectivity resides, at least in part, in stacking interactions between the furonaphthalimide chromophore and DNA base pairs. Since the monomeric compound exhibits a similar selectivity for a GC-rich sequence, but a weaker affinity, we can conclude that the aminoalkyl linker chain essentially serves as a hook to maintain the stability of the drug−DNA complexes and limit the dissociation. The furano ring is likely the principal determinant of GC selectivity for the dimer **MCI3335**, possibly via hydrogen bonding interactions with the amino group of guanine residues within the minor groove. Hydrogen bonding and stacking interactions usually play a

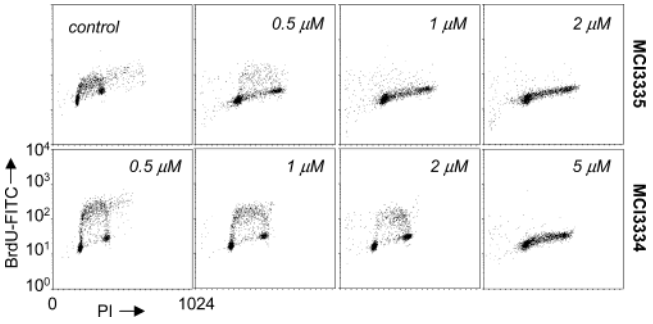

FIGURE 8: Modification of bromodeoxyuridine incorporation in CEM cells treated with **MCI3334** or **MCI3335**. Cells were treated for 24 h with the test drug at the indicated concentrations prior to labeling with the BrdU−FITC conjugate for 1 h and counterstained with propidium iodide (PI).

crucial role in determining DNA sequence-specific reading by bis-intercalators (*59*, *60*).

At this point, it is useful to refer to the antitumor drug DACA and related acridine 4-carboxamide derivatives which behave like the naphthalimides. Crystal structures of different acridine 4-carboxamide−DNA complexes have revealed that three parameters are essential to the formation of very stable complexes at CpG sites: (i) stacking interaction between the tricyclic chromophore and the GC base pairs, (ii) a planar carboxamide group stabilized by an internal H bond and allowing contacts with a proximal DNA phosphate residue via a water bridge, and (iii) H bond interactions between the cationic side chain and the O6 and N7 atoms of guanine in the DNA major groove (*61*−*64*). Much the same parameters can be invoked to explain the similar behavior of the naphthalimide. The reinforced stacking properties of **MCI3335** are expected to contribute to the enhanced temporal stability of the drug−DNA complexes. The imide ring of 9-amino-DACA can be assimilated to the planar H bond-stabilized pseudoring, as illustrated in Figure 10a. This H bond-stabilized conformation, which serves to orient the amino alkyl side chain toward the major groove of DNA, can be formed with either the protonated acridine nitrogen and the C═O group of the adjacent amide bond (Figure 10a) or the nonprotonated neutral form of the N acridine and the NH group of the proximal amide bond (Figure 10b). In each case, the side chain is pushed toward the major groove of DNA which is known to accommodate also the cationic side chain of elinafide (*14*, *15*) and related naphthalene diimides (*65*, *66*). The realization that similar steric and electronic factors control the GC-selective intercalation of acridine 4-carboxamide and modified naphthalimides will be useful in guiding the design of novel dimeric compounds.

Despite its limited capacity to accumulate in the cell nuclei, the dimer **MCI3335** turned out to be considerably more cytotoxic to CEM leukemia cells than the monomer **MCI3334**. Although there is no indication that this can be attributed to the enhanced affinity for DNA per se, it is not uncommon to see a correlation between DNA binding strength and cytotoxicity in the naphthalimide series. Recently, for example, the antiproliferative activity of bisnaphthalimidopropyl polyamine derivatives toward human breast cancer MCF-7 cells was found to be correlated with their binding affinity (*67*). Similar examples have been described with other dimeric intercalators (*68*).

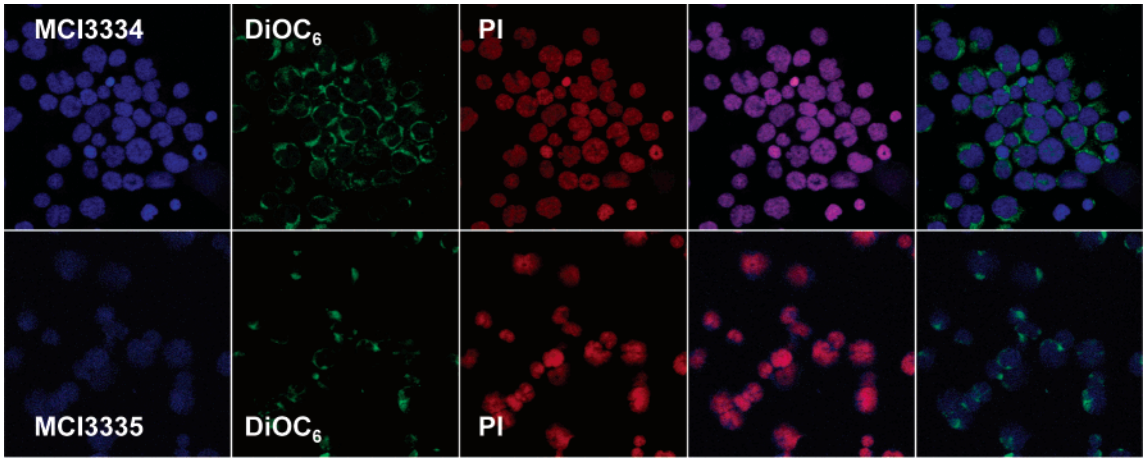

FIGURE 9: Fluorescence micrographs of CEM leukemia cells stained with the indicated compound (20 μM each in blue), with propidium iodide (PI in red), or with 3,3-dihexyloxacarbocyanine iodide ($DiOC_6$ in green). Images on the right side of the figure show the overlay of the naphthalimide compounds with PI (blue and red) or with $DiOC_6$ (blue and green). The cells were incubated with the drug for 4 h, washed, fixed with 2% paraformaldehyde, and then labeled with PI (0.5 μg/mL PI) or $DiOC_6$ (150 nM) prior to the microscopy observation (63×).

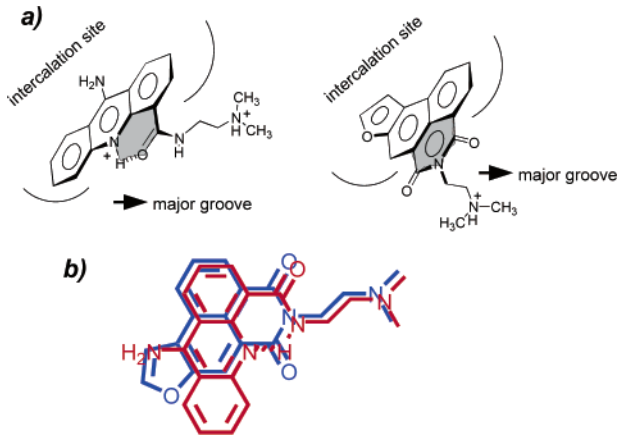

FIGURE 10: (a) Schematic representation of the binding to DNA of the acridine 4-carboxamide derivative (9-amino-DACA) and the furonaphthalimide **MCI3334**. In both cases, the planar chromophore would intercalate between GC base pairs and the appended cationic side chain is directed toward the major groove. The dark ring illustrates the common planar structural motif which is supposed to orient the cationic linker in the same direction. (b) Superimposition of the acridine (red) and naphthalimide (blue) structures. In this case, the acridine nitrogen is shown in its unprotonated form. See the text for more details.

The lack of a poisoning effect of the two test drugs against topoisomerases is surprising and interesting. In particular, the fact that neither **MCI3334** nor **MCI3335** promotes DNA cleavage by topoisomerase II contrasts with the well-documented topoisomerase II poisoning activity exhibited by related monomers such as amonafide and azonafide (*22*, *29*, *30*), and dimers, including elinafide and bisnafide (*7*, *33*). Nevertheless, despite the absence of enzyme inhibition, **MCI3335** is extremely potent at inhibiting the growth of CEM leukemia cells, and the calculated IC_{50} value is even 3 times lower than that measured with elinafide under identical culture conditions (IC_{50} values of 4.9 and 16.5 nM for **MCI3334** and elinafide, respectively). This observation raises questions about the role of topoisomerase II inhibition in the expression of the cytotoxic potential of these bisnaphthalimides. Nitiss and co-workers have concluded that the bisnafide causes cytotoxicity by its action against eukaryotic topoisomerase II. The same conclusion is not valid for the furonaphthalimide derivatives studied here. The mechanism of cell killing by **MCI3335** is a priori topoisomerase II-independent. We are inclined to believe that the loss of the anti-topoisomerase II activity is attributable to the additional heterocyclic ring fused to the naphthalimide system because, in another recent study, we found that tetracyclic bispyrazinonaphthalimides also fail to inhibit topoisomerase II, despite their potent cytotoxic activities. A bispyrazinonaphthalimide derivative [incorporating the same $(CH_2)_2$-NH-$(CH_2)_3$-NH-$(CH_2)_2$ linker as elinafide and **MCI3335**] was found to exhibit promising cytotoxic activities against different cell lines, and this was also associated with a tight bisintercalative binding to DNA, but not to topoisomerase inhibition (*28*). Related to this, it is worth mentioning that similarly, the substitution of the fused furane ring of **MCI3335** for an imidazole ring also provides compounds inactive toward topoisomerase II (unpublished data). Therefore, it may be a general rule that the fusion of a heterocycle to the naphthalene 3 or 4 position abolishes the inhibitory activity of the drugs toward topoisomerase II. In other words, this side of the molecule may be required for interaction with the enzyme or access to the topoisomerase II−DNA interface.

Stacking interactions can be invoked to try to explain the loss of the anti-topoisomerase II seen with **MCI3335**. This bis-tetracyclic compound has a stronger tendency to self-associate than the bis-tricyclic parent molecule elinafide. The increased size of the two planar chromophores must favor a stacking interaction with DNA base pairs, but reinforcing the capacity of the drug to form bis-intercalation complexes may be detrimental to topoisomerase II inhibition. Bisnafide potently inhibits topoisomerase II (*33*), but this compound has appeared to be only a mono-intercalator (*67*). In contrast, elinafide does form bis-intercalation complexes (*14*, *15*) but only weakly inhibits topoisomerase II (*7*). A cytotoxicity study with a pair of Jurkat leukemia cell lines sensitive or resistant to the topoisomerase II inhibitor amsacrine has indicated that elinafide does not exploit topoisomerase II to kill cancer cells. The fusion of the naphthalene moiety with a furane or a pyrazine heterocycle reinforces the stacking properties and the capacity of the drug to intercalate into

DNA, but this is apparently at the expense of topoisomerase II inhibition. Whether other DNA binding enzymes (e.g., helicases, telomerase) are implicated in the cell killing mechanism of **MCI3335** will be the subject of continued examination.

The lack of a poisoning effect of **MCI3335** against topoisomerase II is consistent with the cytometry analysis showing that the dimer does not block cell cycle progression at a specific phase. **MCI3335** inhibits the incorporation of BrdU into newly synthesized DNA. Whether this is linked to DNA binding remains to be determined. Many factors other than the strength of the interaction to the double-stranded DNA bioreceptor combine to influence the potency of a drug in a cellular environment. It remains possible that selective binding of the drug to GC-rich sequences in specific genes represents the initial molecular event which then triggers the cytotoxic activity. DNA is perhaps not the unique but nevertheless is likely the critical biochemical target of **MCI3335** and related bisnaphthalimides. **MCI3335** might be a novel candidate for further preclinical investigations.

ACKNOWLEDGMENT

We thank Mrs. N. Jouy and the IMPRT (IFR114) for access to the BIAcore 3000 instrumentation and Pr. David W. Wilson (Department of Chemistry, Georgia State University, Atlanta, GA) for expert assistance with the SPR experiments. The help of Dr. Zohar Mishal (CNRS, Villejuif, France) for the confocal measurements is acknowledged.

SUPPORTING INFORMATION AVAILABLE

Five figures showing the DNA titrations, the effect of SDS on the absorption and fluorescence spectra of the compounds, thermal denaturation curves, fitting of SPR data, and topoisomerase inhibition. This material is available free of charge via the Internet at http://pubs.acs.org.

REFERENCES

1. Braña, M. F., Castellano, J. M., Morán, M., Pérez de Vega, M. J., Romerdahl, C. R., Qian, X.-D., Bousquet, P., Emling, F., Schlick, E., and Keilhauer, G. (1993) Bis-naphthalimides: a new class of antitumor agents, *Anti-Cancer Drug Des. 8*, 257−268.
2. Braña, M. F., Castellano, J. M., Morán, M., Pérez de Vega, M. J., Perron, D., Conlon, D., Bousquet, P. F., Romerdahl, C. A., and Robinson, S. P. (1996) Bis-naphthalimides 3: Synthesis and antitumor activity of N,N′-bis[2-(1,8-naphthalimido)-ethyl] alkanediamines, *Anti-Cancer Drug Des. 11*, 297−309.
3. Braña, M. F., Cacho, M., Gradillas, A., de Pascual-Teresa, B., and Ramos, A. (2001) Intercalators as anticancer drugs, *Curr. Pharm. Des. 7*, 1745−1780.
4. McRipley, R. J., Burns-Horwitz, P. E., Czerniak, P. M., Diamond, R. J., Diamond, M. A., Miller, J. L. D., Page, R. J., Dexter, D. L., Chen, S.-F., Sun, J. H., Behrens, C. H., Seitz, S. P., and Gross, J. L. (1994) Efficacy of DMP 840: A novel bis-naphthalimide cytotoxic agent with human solid tumor xenograft selectivity, *Cancer Res. 54*, 159−164.
5. Kirshenbaum, M. R., Chen, S.-F., Behrens, C. H., Papp, L. M., Stafford, M. M., Sun, J.-H., Behrens, D. L., Fredericks, J. R., Polkus, S. T., Sipple, P., Patten, A. D., Dexter, D., Seitz, S. P., and Gross, J. L. (1994) (*R*,*R*)-2,2′-[1,2-Ethanediylbis[imino(1-methyl-2,1-ethanediyl)]]-bis[5-nitro-1*H*-benz[de]isoquinoline-1,3-(2*H*)-dione] dimethanesulfonate (DMP 840), a novel bis-naphthalimide with potent nonselective tumoricidal activity *in vitro*, *Cancer Res. 54*, 2199−2206.
6. O'Reilly, S., Baker, S. D., Sartorius, S., Rowinsky, E. K., Finizio, M., Lubiniecki, G. M., Grochow, L. B., Gray, J. E., Pieniaszek, H. J., Jr., and Donehower, R. C. (1998) A phase I and pharmacologic study of DMP 840 administered by 24-hour infusion, *Ann. Oncol. 9*, 101−104.
7. Bousquet, P. F., Braña, M. F., Conlon, D., Fitzgerald, K. M., Perron, D., Cocchiaro, C., Miller, R., Moran, M., George, J., Qian, X.-D., Keilhauer, G., and Romerdahl, C. A. (1995) Preclinical evaluation of LU 79553: a novel bisnaphthalimide with potent antitumor activity, *Cancer Res. 55*, 1176−1180.
8. Cobb, P. W., Degen, D. R., Clark, G. M., Chen, S. F., Kuhn, J. G., Gross, J. L., Kirshenbaum, M. R., Sun, J. H., Burris, H. A., and Von Hoff, D. D. (1994) Activity of DMP840, a new bis-naphthalimide, on primary human tumor colony-forming units, *J. Natl. Cancer Inst. 5*, 1462−1465.
9. Houghton, P. J., Cheshire, P. J., Hallman, J. C., Gross, J. L., McRipley, R. J., Sun, J. H., Behrens, C. H., Dexter, D. L., and Houghton, J. A. (1994) Evaluation of a novel bis-naphthalimide anticancer agent, DMP840, against human xenografts derived from adult, juvenile, and pediatric cancers, *Cancer Chemother. Pharmacol. 33*, 265−272.
10. LoRusso, P., Demchik, L., Dan, M., Polin, L., Gross, J. L., and Corbett, T. H. (1995) Comparative efficacy of DMP 840 against mouse and human solid tumor models, *Invest. New Drugs 13*, 195−203.
11. Thompson, J., Pratt, C. B., Stewart, C. F., Avery, L., Bowman, L., Zamboni, W. C., and Pappo, A. (1998) Phase I study of DMP840 in pediatric patients with refractory solid tumors, *Invest. New Drugs 16*, 45−49.
12. Villalona-Calero, M. A., Eder, J. P., Toppmeyer, D. L., Allen, L. F., Fram, R., Velagapudi, R., Myers, M., Amato, A., Kagen-Hallet, K., Razvillas, B., Kufe, D. W., Von Hoff, D. D., and Rowinsky, E. K. (2001) Phase I and pharmacokinetic study of LU79553, a DNA intercalating bisnaphthalimide, in patients with solid malignancies, *J. Clin. Oncol. 19*, 857−869.
13. Gamage, S. A., Spicer, J. A., Finlay, G. J., Stewart, A. J., Charlton, P., Baguley, B. C., and Denny, W. A. (2001) Dicationic bis(9-methylphenazine-1-carboxamides): relationships between biological activity and linker chain structure for a series of potent topoisomerase targeted anticancer drugs, *J. Med. Chem. 44*, 1407−1415.
14. Bailly, C., Braña, M., and Waring, M. J. (1996) Sequence-selective intercalation of antitumour bisnaphthalimides into DNA. Evidence for an approach via the major groove, *Eur. J. Biochem. 240*, 195−208.
15. Gallego, J., and Reid, B. R. (1999) Solution structure and dynamics of a complex between DNA and the antitumor bisnaphthalimide LU-79553: intercalated ring flipping on the millisecond time scale, *Biochemistry 38*, 15104−15115.
16. Wright, R. G. McR., Wakelin, L. P. G., Fieldes, A., Acheson, R. M., and Waring, M. J. (1980) Effects of ring substituents and linker chains on the bifunctional intercalation of diacridines into deoxyribonucleic acid, *Biochemistry 19*, 5825−5836.
17. Costanza, M. E., Berry, D., Henderson, I. C., Ratain, M. J., Wu, K., Shapiro, C., Duggan, D., Kalra, J., Berkowitz, I., and Lyss, A. P. (1995) Amonafide: An active agent in the treatment of previously untreated advanced breast cancer: a cancer and leukemia group B study (CALGB 8642), *Clin. Cancer Res. 1*, 699−704.
18. Costanza, M. E., Weiss, R. B., Henderson, I. C., Norton, L., and Berry, D. A., Cirrincione, C., Winer, E., Wood, W. C., Frei, E., McIntyre, O. R., and Schilsky, R. L. (1999) Safety and efficacy of using a single agent or a phase II agent before instituting standard combination chemotherapy in previously untreated metastatic breast cancer patients: report of a randomized study: Cancer and Leukemia Group B 8642, *J. Clin. Oncol. 17*, 1397−1406.
19. Kreis, W., Chan, K., Budman, D. R., Allen, S. L., Fusco, D., Mittelman, A., Hock, K., Akerman, S., Calabro, A., Puccio, C., and Spigelman, M. (1996) Clinical pharmacokinetics of amonafide (NSC 308847) in 62 patients, *Cancer Invest. 14*, 320−327.
20. Witte, R. S., Hsieh, P., Elson, P., Oken, M. M., and Trump, D. L. (1996) A phase II trial of amonafide, caracemide, and homoharringtonine in the treatment of patients with advanced renal cell cancer, *Invest. New Drugs 14*, 409−413.
21. Leaf, A. N., Neuberg, D., Schwartz, E. L., Wadler, S., Ritch, P. S., Dutcher, J. P., and Adams, G. L. (1997) An ECOG phase II study of amonafide in unresectable or recurrent carcinoma of the head and neck (PB390). Eastern Cooperative Oncology Group, *Invest. New Drugs 15*, 165−172.
22. Mayr, C. A., Sami, S. M., and Dorr, R. T. (1997) In vitro cytotoxicity and DNA damage production in Chinese hamster

ovary cells and topoisomerase II inhibition by 2-[2′-(dimethylamino)ethyl]-1,2-dihydro-3H-dibenz[de,h]isoquinoline-1,3-diones with substitutions at the 6 and 7 positions (azonafides), *Anticancer Drugs 8*, 245−256.
23. Sami, S. M., Dorr, R. T., Alberts, D. S., Solyom, A. M., and Remers, W. A. (2000) Analogues of amonafide and azonafide with novel ring systems, *J. Med. Chem. 43*, 3067−3073.
24. Bear, S., and Remers, W. A. (1996) Computer simulation of the binding of amonafide and azonafide to DNA, *J. Comput.-Aided Mol. Des. 10*, 165−175.
25. Braña, M. F., Castellano, J. M., Moran, M., Emling, F., Kluge, M., Schlick, E., Klebe, G., and Walker, N. (1995) Synthesis, structure and antitumor activity of new benz[d,e]isoquinoline-1,3-diones, *Arzneim.-Forsch. 45*, 1311−1318.
26. Braña, M. F., Castellano, J. M., Perron, D., Maher, C., Conlon, D., Bousquet, P. F., George, J., Qian, X. D., and Robinson, S. P. (1997) Chromophore-modified bis-naphthalimides: synthesis and antitumor activity of bis-dibenz[de,h]isoquinoline-1,3-diones, *J. Med. Chem. 40*, 449−454.
27. Braña, M. F., Cacho, M., García, M. A., Pascual-Teresa, B., Ramos, A., Acero, N., Llinares, F., Muñoz-Mingarro, D., Abradelo, C., Rey-Stolle, M.-F., and Yuste, M. (2002) Synthesis, antiumor activity, molecular modeling, and DNA binding properties of a new series of imidazonaphthalimides, *J. Med. Chem. 45*, 5813−5816.
28. Braña, M. F., Cacho, M., Ramos, A., Dominguez, M. T., Pozuelo, J. M., Abradelo, C., Rey-Stolle, M. F., Yuste, M., Carrasco, C., and Bailly, C. (2003) Synthesis, biological evaluation and DNA binding properties of novel mono- and bisnaphthalimides, *Org. Biomol. Chem. 1*, 648−654.
29. Hsiang, Y. H., and Liu, L. F. (1989) Topoisomerase II-mediated DNA cleavge by amonafide and its structural analogs, *Mol. Pharmacol. 36*, 371−376.
30. De Isabella, P., Zunino, F., and Capranico, G. (1995) Base sequence determinants of amonafide stimulation of topoisomerase II DNA cleavage, *Nucleic Acids Res. 23*, 223−229.
31. Borgnetto, M. E., Zunino, F., Tinelli, S., Käs, E., and Capranico, G. (1996) Drug-specific sites of topoisomerase II DNA cleavage in Drosophila chromatin. Heterogeneous localization and reversibility, *Cancer Res. 56*, 1855−1862.
32. Slunt, K. M., Grace, J. M., McDonald, T. L., and Pearson, R. D. (1996) Effect of mitonafide analogs on topoisomerase II of *Leishmania chagasi*, *Antimicrob. Agents Chemother. 40*, 706−709.
33. Nitiss, J. L., Zhou, J., Rose, A., Hsiung, Y., Gale, K. C., and Osheroff, N. (1998) The bis(naphthalimide) DMP-840 causes cytotoxicity by its action against eukaryotic topoisomerase II, *Biochemistry 37*, 3078−3085.
34. Waring, M. J., Gonzalez, A., Jimenez, A., and Vazquez, D. (1979) Intercalative binding to DNA of antitumour drugs derives from 3-nitro-1,8-naphthalic acid, *Nucleic Acids Res. 7*, 217−229.
35. Patten, A., Pacofsky, G., Seitz, S., Akamike Emeka, A., Cherney, R., Kaltenbach, R., III, and Orwat, M. (1995) Polycyclic and Heterocyclic Chromophores for Bis-imide Tumoricidals, WO Patent 9,500,490.
36. Davis, T. M., and Wilson, W. D. (2000) Determination of the refractive index increments of small molecules for correction of surface plasmon resonance data, *Anal. Biochem. 284*, 348−353.
37. Davis, T. M., and Wilson, W. D. (2001) Surface plasmon resonance biosensor analysis of RNA-small molecule interactions, *Methods Enzymol. 340*, 22−51.
38. Connors, K. A. (1987) *Binding Constants*, Wiley, New York.
39. Houssier, C. (1981) Investigating nucleic acids, nucleoproteins, polynucleotides, and their interactions with small ligands by electro-optical systems, in *Molecular Electro-Optics* (Krause, S., Ed.) pp 363−398, Plenum Publishing Corp., New York.
40. Houssier, C., and O'Konski, C. T. (1981) Electro-optical instrumentation systems with their data acquisiton and treatment, in *Molecular Electro-Optics* (Krause, S., Ed.) pp 309−339, Plenum Publishing Corp., New York.
41. Colson, P., Bailly, C., and Houssier, C. (1996) Electric linear dichroism as a new tool to study sequence preference in drug binding to DNA, *Biophys. Chem. 58*, 125−140.
42. Bailly, C. (2001) DNA relaxation and cleavage assays to study topoisomerase I inhibitors, *Methods Enzymol. 340*, 610−623.
43. Lavesa, M., and Fox, K. R. (2001) Preferred binding sites for [N-MeCYs(3),N-MeCys(7)]TANDEM determined using a universal footprinting substrate, *Anal. Biochem. 293*, 246−250.
44. Bailly, C., and Waring, M. J. (1995) Comparison of different footprinting methodologies for detecting binding sites for a small ligand on DNA, *J. Biomol. Struct. Dyn. 12*, 869−898.
45. Gough, A. N., Jones, R. L., and Wilson, W. D. (1979) Dimerization of coralyne and its propyl analogue and their association with DNA, *J. Med. Chem. 22*, 1551−1554.
46. Nguyen, B., Tardy, C., Bailly, C., Colson, P., Houssier, C., Kumar, A., Boykin, D. W., and Wilson, W. D. (2002) Influence of compound structure on affinity, sequence selectivity and mode of binding to DNA for unfused aromatic dications related to furamidine, *Biopolymers 63*, 281−297.
47. Fox, K. R., and Waring, M. J. (2001) High-resolution footprinting studies of drug−DNA complexes using chemical and enzymic probes, *Methods Enzymol. 340*, 412−430.
48. Lansiaux, A., Dassonneville, L., Facompre, M., Kumar, A., Stephens, C. E., Bajic, M., Tanious, F., Wilson, W. D., Boykin, D. W., and Bailly, C. (2002) Distribution of furamidine analogues in tumor cells: influence of the number of positive charges, *J. Med. Chem. 45*, 1994−2002.
49. Lansiaux, A., Tanious, F., Mishal, Z., Dassonneville, L., Kumar, A., Stephens, C. E., Hu, O., Wilson, W. D., Boykin, D. W., and Bailly, C. (2002) Distribution of furamidine analogues in tumor cells: Targeting of the nucleus or mitochondria depending on the amidine substitution, *Cancer Res. 62*, 7219−7229.
50. Charmantray, F., Demeunynck, M., Carrez, D., Croisy, A., Lansiaux, A., Bailly, C., and Colson, P. (2003) 4-Hydroxymethyl-3-aminoacridine derivatives as a new family of anticancer agents, *J. Med. Chem. 46*, 967−977.
51. Wilson, W. D. (2002) Analyzing biomolecular interactions, *Science 295*, 2103−2105.
52. Lacy, E. R., Madsen, E. M., Lee, M., and Wilson, W. D. (2003) Polyamide dimer stacking in the DNA minor groove and recognition of T·G mismatched base pairs in DNA, in *Small Molecule DNA and RNA Binders* (Demeunynck, M., Bailly, C., and Wilson, W. D., Eds.) Vol. 2, pp 384−413, Wiley-VCH, New York.
53. Carrasco, C., Vezin, H., Wilson, W. D., Ren, J., Chaires, J. B., and Bailly, C. (2002) DNA binding properties of the indolocarbazole antitumor drug NB-506, *Anti-Cancer Drug Des. 16*, 99−107.
54. Carrasco, C., Facompré, M., Chisholm, J. D., Van Vranken, D. L., Wilson, W. D., and Bailly, C. (2002) DNA sequence recognition by the indolocarbazole antitumor antibiotic AT2433-B1 and its diastereoisomer, *Nucleic Acids Res. 30*, 1774−1781.
55. Boger, D. L., and Saionz, K. W. (1999) DNA binding properties of key sandramycin analogues: Systematic examination of the intercalation chromophore, *Bioorg. Med. Chem. 7*, 315−321.
56. Carrasco, C., Rosu, F., Gabelica, V., Houssier, C., De Pauw, E., Garbay-Gaureguiberry, C., Roques, B., Wilson, W. D., Chaires, J. B., Waring, M. J., and Bailly, C. (2002) Tight binding of the antitumor drug ditercalinium to quadruplex DNA, *ChemBioChem 3*, 1235−1241.
57. Bailly, C., Denny, W. A., Mellor, L., Wakelin, L. P. G., and Waring, M. J. (1992) Sequence-specificity of the binding of 9-aminoacridine- and amsacrine-4-carboxamides to DNA studied by DNase I footprinting, *Biochemistry 31*, 3514−3524.
58. Blanchard, S., Rodriguez, I., Tardy, C., Baldeyrou, B., Bailly, C., Colson, P., Houssier, C., Pfeiffer, B., Renard, P., Caubère, P., and Guillaumet, G. (2002) Synthesis of mono- and bis-dihydrodipyridopyrazines and assessment of their DNA binding and cytotoxic properties, manuscript in preparation.
59. Gallego, J., Luque, F. J., Orozco, M., Burgos, C., Alvares-Builla, J., Rodrigo, M. M., and Gago, F. (1994) DNA sequence-specific reading by echinomycin: role of hydrogen bonding and stacking interactions, *J. Med. Chem. 37*, 1602−1609.
60. Gago, F. (1998) Stacking interactions and intercalative DNA binding, *Methods 14*, 277−292.
61. Tood, A. K., Adams, A., Thorpe, J. H., Denny, W. A., Wakelin, L. P. G., and Cardin, C. J. (1999) Major groove binding and DNA-induced fit in the intercalation of a derivative of the mixed topoisomerase I/II poison N-(2-(dimethylamino)ethyl)acridine-4-carboxamide (DACA) into DNA: X-ray structure complexed to $d(CG(5\text{-}BrU)ACG)_2$ at 1.3 Å resolution, *J. Med. Chem. 42*, 536−540.
62. Adams, A., Guss, J. M., Collyer, C. A., Denny, W. A., and Wakelin, L. P. G. (1999) Crystal structure of the topoisomerase II poison 9-amino-[*N*-(2-dimethylamino)ethyl]acridine-4-carboxamide bound to the DNA hexanucleotide $d(CGTACG)_2$, *Biochemistry 38*, 9221−9233.

63. Adams, A., Guss, J. M., Collyer, C. A., Denny, W. A., Prakash, A. S., and Wakelin, L. P. G. (2000) Crystal structure of 9-amino-(*N*-[2-(4-morpholinyl)ethyl])-4-acridinecarboxamide bound to d(CG-TACG)$_2$: implications for structure−activity relationships of acridinecarboxamide topoisomerase poisons, *Nucleic Acids Res. 30*, 719−725.
64. Adams, A., Guss, J. M., Collyer, C. A., Denny, W. A., Prakash, A. S., and Wakelin, L. P. G. (2000) Acridinecarboxamide topoisomerase poisons: Structural and kinetic studies of the DNA complexes of 5-substituted 9-amino-(*N*-(2-dimethylamino)ethyl)-acridine-4-carboxamides, *Mol. Pharmacol. 58*, 649−658.
65. Lokey, R. S., Kwok, Y., Guelev, V., Pursell, C. J., Hurley, L. H., and Iverson, B. L. (1997) A new class of polyintercalating molecules, *J. Am. Chem. Soc. 119*, 7202−7210.
66. Guelev, V., Lee, J., Ward, J., Sorey, S., Hoffman, D. W., and Iverson, B. L. (2001) Peptide bis-intercalator binds DNA via threading mode with sequence specific contacts in the major groove, *Chem. Biol. 8*, 415−425.
67. Pavlov, V., Kong Thoo Lin, P., and Rodilla, V. (2001) Cytotoxicity, DNA binding and localisation of novel bis-naphthalimidopropyl polyamine derivatives, *Chem.-Biol. Interact. 137*, 15−24.
68. Spicer, J. A., Gamage, S. A., Finlay, G. J., and Denny, W. A. (2002) Synthesis and evaluation of unsymmetrical bis(arylcarboxamides) designed as topoisomerase-targeted anticancer drugs, *Bioorg. Med. Chem. 10*, 19−29.
69. Cherney, R. J., Swartz, S. G., Patten, A. D., Akamike, E., Sun, J. H., Kaltenbach, R. F., III, Seit, S. P., Behrens, C. H., Getahun, Z., Trainor, G. L., Vavala, M., Kirshenbaum, M. R., Papp, L. M., Stafford, M. P., Czerniak, P. M., Diamond, R. J., McRipley, R. J., Page, R. J., and Gross, J. L. (1997) The synthesis and antitumor evaluaion of unsymmetrical bis-imides, *Bioorg. Med. Chem. Lett. 7*, 163−168.

BI027415C